https://doi.org/10.26552/com.C.2019.2.58-68

Vladimir Kindl - Miroslav Byrtus - Bohumil Skala - Vaclav Kus*

KEY ASSEMBLING ISSUES RELATING TO MECHANICAL VIBRATION OF FABRICATED ROTOR OF LARGE INDUCTION MACHINES

In many applications, where rotating machines of high power are used, high demands on reliability and safety are laid. Precise manufacturing procedures has to be kept even in case of machines retrofits when e.g. rotors are newly assembled. Even small inaccuracies or misguiding the precise technological procedure can lead to improper running of the machine and it can result in shut-down of complete drive. In case of primary circuits of nuclear power plants, it further means the shut-down of the whole power plant. Consequently, it results in significant financial losses (foregone profit and cost given by problem fixing). The paper presents a methodology of vibration origin investigation in case of large rotating machines which are part of drives like pump, compressors etc. The methodology is based on the detection of undesirable vibration using a diagnostic system on-site and further it uses mathematical modelling of corresponding mechanical parts to reveal the vibration origin. The modelling along with the measurement showed that the detected dangerous vibration is caused by misguided assembling of the rotor of the machine.

Keywords: *induction, machine, rotor, vibration, unbalance, assembling*

1. Introduction

Not only the industry but the whole today's society is virtually dependent on a continuous supply of electric energy. With the electricity our work is easier which increases the comfort of our lives and gives us a sense of safety. A smooth operation of power plant is therefore very important aspect for a successful and continuous development of our civilization.

Key function elements of conventional thermal, nuclear, and hydroelectric power plants are rotating electrical machines. Besides the power generator the power plant utilizes a large amount of supporting drives (conveyors, pushers, ...) and auxiliary systems (mills, pumps, ...), which together form a huge functional unit. Even a brief function drop-out of any auxiliary system may lead to incidental power plant downtime and thus the power outage.

The power plant operation puts very high operational demands on machines, especially in terms of wide range of dynamic loads. Therefore, it is very important to regularly monitor the vibration of the machines and perform any maintenance earlier than necessary and as planned. This is particularly relevant to large power machines whose rotors have a complicated structure.

One of the major properties of electric machine rotors is their mechanical stiffness [1-6]. Rotors must resist mechanical stress, which primarily comprises centrifugal forces, rotor vibrations, thermal dilatation and the interference press fit [7-12]. In addition to tangential forces producing the machine torque, rotors are also affected by electromagnetic forces in a radial direction [13-18]. These forces gain much higher amplitudes, but they are mutually cancelled [19-21] due to the symmetric mounting of the rotor. If this symmetry is destroyed, for instance, as a result of faulty balancing of the rotor or its eccentric mounting, a unilateral magnetic force occurs [22].

In motors of small dimensions, whose diameter hardly exceeds one meter, the rotor magnetic circuits can be punched from a single sheet. In such a case, the issue of clamping forces can be ignored [23-25]. With a segment layout of rotor laminations, the sufficient clamping force must be achieved by a design with a proper number of clamping bolts, their proper diameter and position taking into account the magnetic flux and saturation of the magnetic circuit.

Rotors of large diameters constitute a different situation. In this case, the number, size and location of the holes for clamping bolts are not critical. The size of the magnetic yoke makes the design trouble-free. The major problem, however, is the size of the mass rotating along the large diameter of the rotor. This leads to substantial centrifugal forces and to the necessity of large friction forces between the individual lamination segments. The necessary friction force is achieved by a large clamping pressure. The maximum value of the clamping force is predominantly limited by the stiffness in the area of ventilation ducts. If the clamping force is insufficient, the segments are loosened, which leads to an imbalance of the rotor. A small clamping force results in loosened ventilation sheets and their shift to the ventilation gap.

The aim of the article is to present a methodology of determining the source of vibration of large machines. The methodology is based on on-site vibration measurement and on analysis of related phenomena like rotor-stator dynamics, analysis of material stress and clamping force of the rotor packet. Other works relating to rotor vibration can be followed in [25-37].

In many applications, only the vibration measurement, which is usually part of a diagnostic system, is presented.

* **Vladimir Kindl, Miroslav Byrtus, Bohumil Skala, Vaclav Kus**
University of West Bohemia, Faculty of Electrical Engineering, RICE, Pilsen, Czech Republic
E-mail: vkindl@rice.zcu.cz

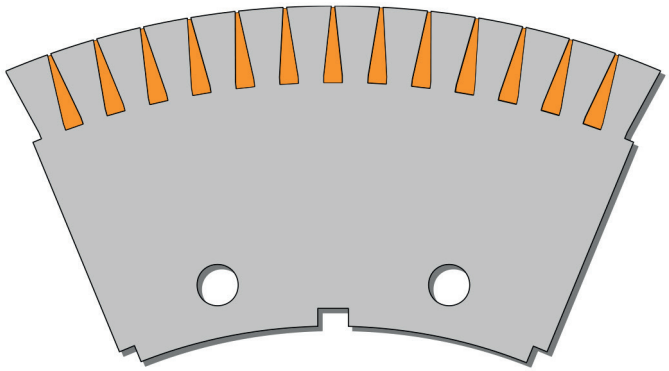

Figure 1 *Annular ring segment of a large asynchronous machine*

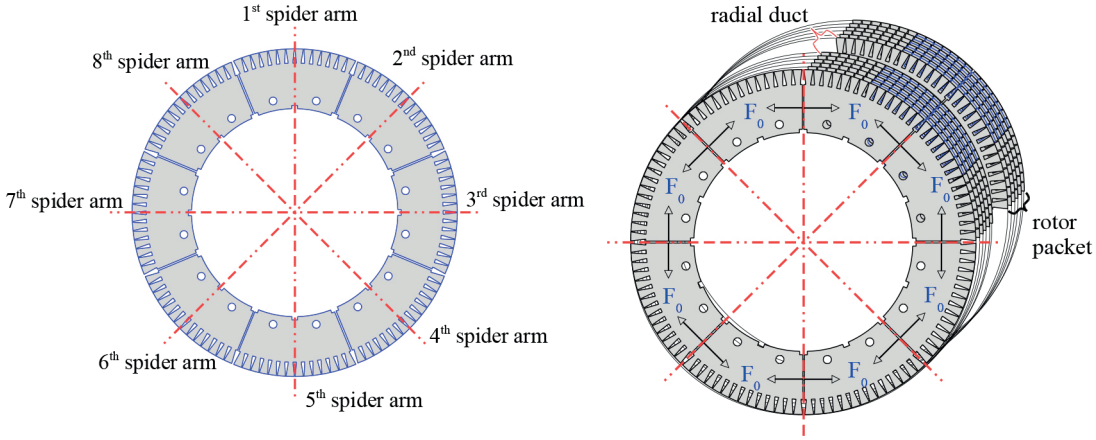

Figure 2 *Rotor packed mounted on the spider arms - odd lamination layer on the left side and even lamination layer on the right side*

The diagnostics can only determine whether the vibration is acceptable or not, since the methodology presented here goes behind and tries to propose a particular procedure for the vibration origin determination.

2. Rotor packet assembling design

A rotor stack is assembled by stacking up steel laminations (see Figure 1). In a steady-state, a magnetic flux with a slip frequency (fractions of Hz up to several Hz) passes through the rotor. However, during the rotor run-up or during a more significant load, the frequency is large and the iron core losses are higher. Therefore, a laminated structure of rotors is necessary.

A rotor stack with a diameter larger than one meter is assembled by stacking up annular segmented steel ring. All odd lamination layers are stacked to even lamination layers with a half overlap (see Figure 2). During assembling, the segments are put on the clamping bolts through the punched-out holes.

Rotor stack is constructed with diameter smaller than the diameter of the rotor spider. Then it is mounted on the rotor spider with an overlap achieved by heating up the lamination, or this method can be combined with super-cooling of the rotor spider with liquid nitrogen. This gives rise to significant radial force acting on the rotor even if it is stopped.

Figure 2 clearly shows that every even layer of lamination is forced to gape in the direction from the radial wedges on the spider arms. This is a serious design error which increases the peripheral stress of the lamination ring by the F_o force. The size of the segments is influenced by many factors [22]. The technological clearance between the sheets in one layer within the contact plane is usually around 0.5 mm. After compression with the relevant pressure, the rotor stack is clamped with clamping rings and bolts. The bolts must exert a sufficient clamping force, thus creating a pre-stressed bolted joint.

Apart from mechanical forces, other forces are also acting in the rotor, namely electromagnetic forces, dynamic forces and forces caused by thermal dilatation [22-24].

3. Requirements for bolts tightening torque

Loosening of a lamination segment is prevented by the friction force between the sheets which is exerted by the clamping pressure. This pressure is created by continuous pressure on the lamination stack as early as during the rotor manufacture. In order to prevent a drop in this pressure as a result of vibrations during the motor operation, the entire rotor pack is clamped with bolts, thus creating a pre-stressed bolted joint. The nuts on the bolts must be tightened with a relevant tightening torque and secured with a weld to prevent loosening.

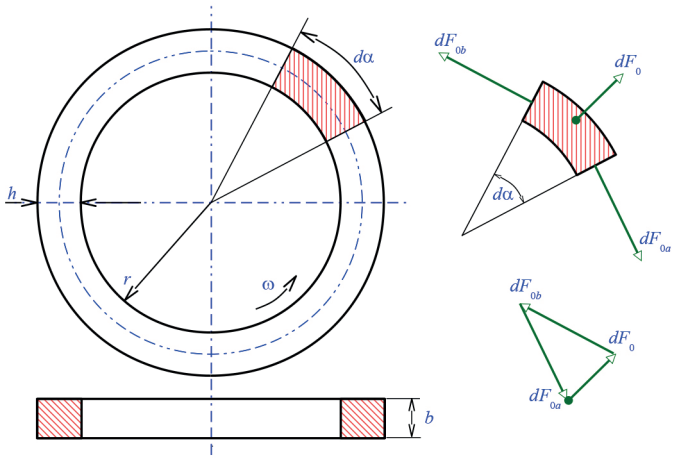

Figure 3 *Forces acting in rotating ring*

If the friction specified above is not sufficient, lamination segments are loosened and the bolts experience both tensile stress and bending stress. This has a negative impact on the rotor dynamics.

The allowable tightening torque of the bolts themselves is from the mechanical point of view many times greater, which means that the mechanical potentialities of bolts are not fully utilized. Their task is completely different - namely to ensure an even clamping pressure along the entire perimeter. According to the required clamping pressure, the number of clamping bolts is determined. However, although the clamping pressure must make the stack compact, it should not be too intense, as it could cause a collapse of ventilation spacers. The stack can be mounted onto the rotor spider in two ways.

First, by attachment with an interference press fit, where the clamping force between the spider arm and the rotor stack will ensure fixing in radial direction. The torque is transferred via tangential wedges because the clamping itself does not exert any additional friction force able to transfer the torque.

Second, by attachment without an interference press fit. Tangential wedges are used for the same reason as above. However, the pack is not secured in the radial direction. This paradoxically increases the need for a greater tightening torque of the bolts.

The large tightening torque is necessary in order to achieve the resistance of the pack to dynamic shocks. During the rotor operation, clearances sometimes occur as a result of various thermal dilatations of the spider arms and the rotor stack. If the structural clamp of the laminations is insufficient and their shift within the stack occurs, the rotor becomes unbalanced and vibrations occur. These vibrations are a further and much stronger source of dynamic forces, which then, in turn, affect the stack lamination (known as additive feedback). Therefore, the calculation of the tightening torque of bolts is the key factor affecting the reliability of operation of large rotors.

4. Analysis of clamping forces

Rotors of large rotating machines are usually operated at a constant speed. With respect to rotor stack dimensions, the effects of field of centrifugal forces cannot be neglected. Moreover, it is a significant source of mechanical loads. The magnitude of clamping force has to take into account the way how the stack segments are fixed to each other.

4.1 First insight calculation

Let us assume, the rotor rotates with an operational speed ω. Further let us suppose a ring with radius r and height h (see Figure 3). Let us consider an infinitesimal small element of mass dm wich corresponds with an angular sector which is given by angle da. The magnitude of the centrifugal force acting on the assumed element can be then expressed in following form

$$dF_o = \omega^2\left(r+\frac{h}{2}\right)dm \approx \omega^2 r^2 \rho b h d\alpha\,. \tag{1}$$

The effect of centrifugal dF_o has to be balanced by inner circumferential tensile forces F_{oa} and F_{ob}, which are of the same size. As for the size of the elementary force dF_o, the following must hold

$$dF_o = Fd\alpha\,. \tag{2}$$

Comparing Equations (1) and (2), one can arrive to the expression of the inner tensile force

$$F = \omega^2 r^2 \rho b h\,, \tag{3}$$

which causes inner tensile stress

$$\sigma = {}^{F}\!/_{bh} = \omega^2 r^2 \rho\,. \tag{4}$$

The centrifugal forces will cause the circumference of the revolving ring to increase. In order to calculate the relative lengthening, the Hook Law can be used, in which the following holds

$$\varepsilon = \frac{2\pi(r+\Delta r)-2\pi r}{2\pi r} = \frac{\Delta r}{r} = \frac{\sigma}{E} = \frac{\omega^2\rho}{E}r^2 \tag{5}$$

The increase in the radius of the rotating ring is expressed after rearrangements as follows

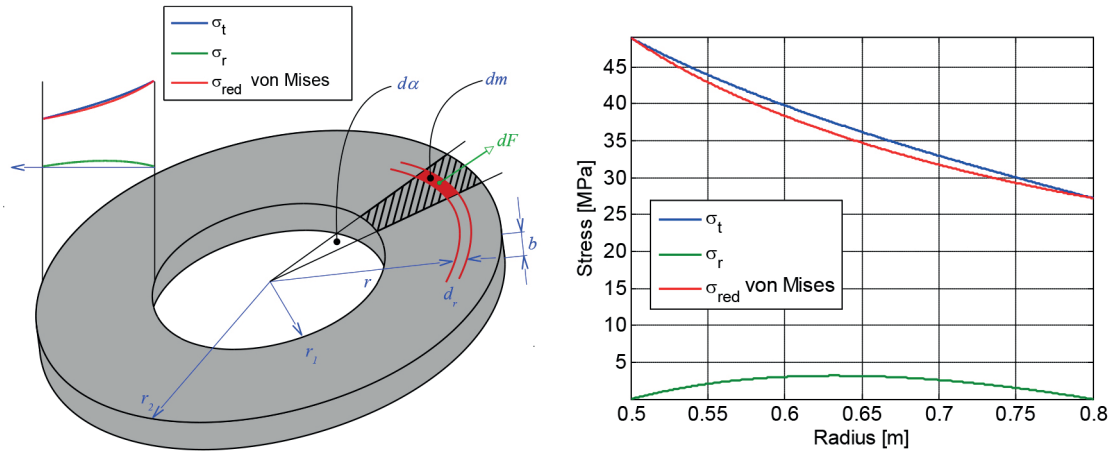

Figure 4 *Stress analysis of the rotating ring corresponding to the rotor packet*

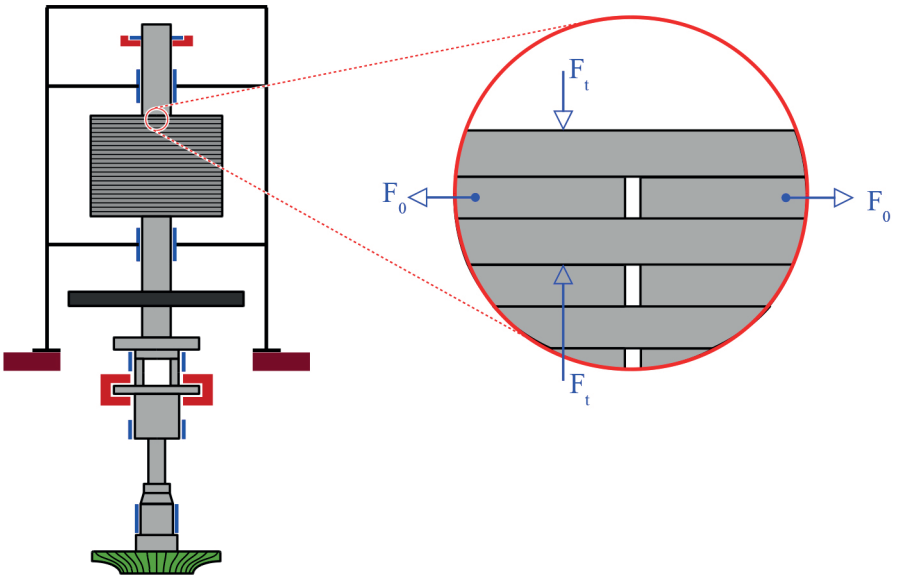

Figure 5 *Friction force and tensile force per partial lamination segments*

Table 1 *Tensile force*

Calculation approach	Tensile force [MN]	Tensile stress [MPa]
First inside approach	16.08	47
Using stress analysis	12.94 (integral value)	depends on the radial position
Data given by manufacturer	17.49	5.33

$$\Delta r = \frac{\omega^2 \rho}{E} r^3 . \tag{6}$$

This increase of the radius results in the decrease of the interference fit and the decrease in the clamping force across the spider arms.

4.2 Calculation using stress analysis

Further, the rotating rotor packet can be considered as a rotating ring loaded by centrifugal force F, which causes following two principal stresses

$$\sigma_r(r) = D_1 - \frac{D_2}{r_2} - (3+\nu)\frac{\rho\omega^2}{8} r^2, \tag{7}$$

$$\sigma_t(r) = D_1 - \frac{D_2}{r_2} - (1+3\nu)\frac{\rho\omega^2}{8} r^2, \tag{8}$$

where $\sigma_r(r)$ stands for radial stress and $\sigma_t(r)$ for tensile stress in the ring. These two quantities are dependent on the radial position r [37]. Considering the nominal speed of the investigated machine, the particular values of the stresses (see Table 1) are presented in Figure 4 along with the ring view. To determine the stresses, an infinitesimal element of the ring is used to formulate a general stress equilibrium. Details can be found in [37].

The manufacturer used an approach for clamping force determination which led to values presented in Table 2. The quantities seem to have inadequate values. They are insufficient to guarantee to compactness of the rotor during its operation.

Table 2 *Clamping force determination*

Calculation approach	Clamping force [kN]	Used bold capacity [%]
First inside approach	166.7	47
Using stress analysis	164.7	46.7
Data given by manufacturer	86.2	24.4

Figure 6 *Plastic distortion of the ventilation sheet (see the upper hole)*

5. Clamping pressure determination

As bolts must not be subjected to shear stress, the tensile force given by Equation (7) can be transferred by friction forces between lamination layers only. The friction coefficient between varnished sheets has usually a value of μ = 0.1. As the number of lamination layers is known, it is possible to determine the tensile force per one overlap of the layer (Figure 5).

The necessary clamping force is expressed as

$$F_T = \frac{2F_O}{\mu}, \tag{9}$$

and the corresponding clamping pressure as

$$p = 2\frac{F_T}{S_S}, \tag{10}$$

where S_s signifies the surface area of one lamination segment.

The tightening torque allowed across the M_{36} bolt is M_{36}=2456 Nm, which would exert the clamping force F_{36}=352.87 kN in the bolt. The bolts capacity that will be used, can be determined as

$$\eta_{36} = \frac{F_T}{F_{36}} \tag{11}$$

6. Stress analysis of a rotor packet segment in centrifugal force field

After rotor disassembling, a distortion of the ventilation sheets has been found (Figure 6). To investigate where the origin of the distortion is, a limit case has been considered, i.e. it has been assumed that the ventilation sheet is not fixed by clamping force and is loaded by the field of centrifugal forces.

This case was modelled by finite element model and the stress analysis was performed. From the results, it can be seen that, if there is almost none clamping force, a radial shift of laminations and a plastic distortion around the bolt occur. Figure 7 clearly shows that in the critical areas, the stress exceeds the value yield strength.

7. Eccentricity due to rotor packet segment sliding

Based on the finding presented above, the mechanism of eccentricity is caused by rotor segment sliding due to insufficient rotor packet clamping. As presented in Figure 8, there are two possibilities of the segment releasing: the first comprises two segment releasing (Figure 8 left), the second lies in releasing of three segment (Figure 8 right). These two mechanisms are coupled and arise mutually.

The resulting value of imbalance of the rotor packet was determined based on the estimate of the shift of the segments. The shift is supposed to be 1mm radially into the ventilation gap of the machine.

8. Vibration source detection in a circulating pump drive

The objective was to design the model of the machine in such a way that it could be used to determine the size of vibrations. Here the source of vibrations is the loosening of several segments and their radial shift leading to an imbalance. This imbalance is further affected by a unilateral magnetic pull which causes a further increase in vibrations. The model must be able to simulate an arbitrary imbalance in any spot of the rotor (see Figure 3). The model takes into account the basic properties of a stator as well.

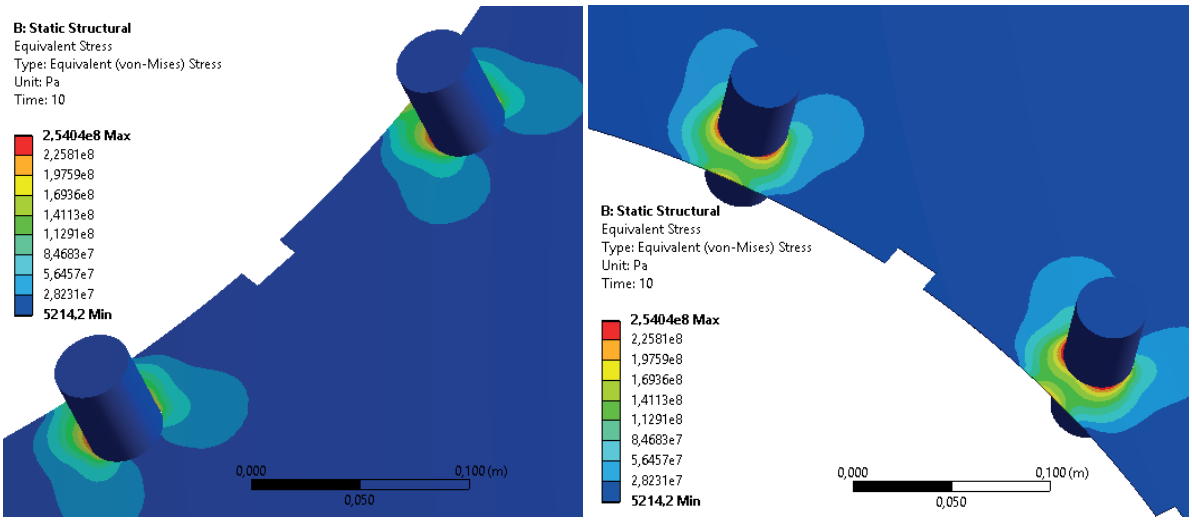

Figure 7 *Simulation of the stress applied to the ventilation sheet due to centrifugal forces*

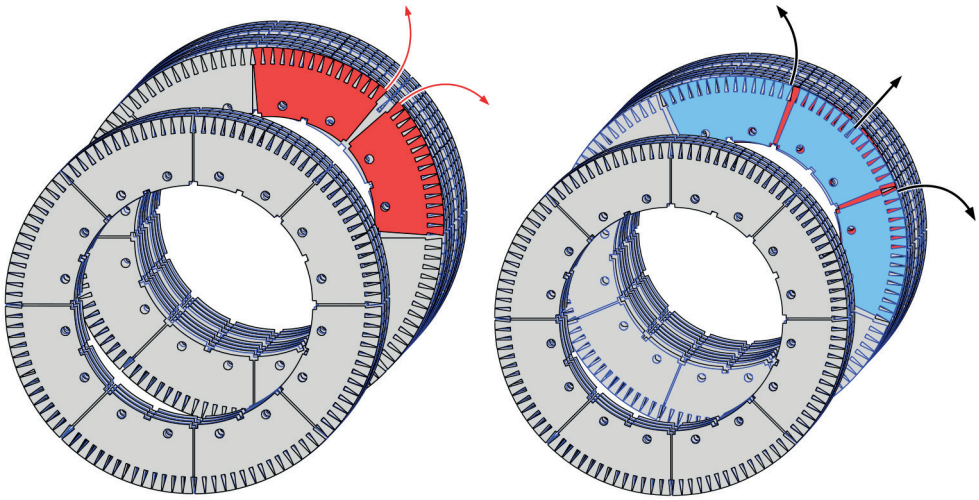

Figure 8 *The mechanism of eccentricity origin - even and odd segments releasing*

8.1 Dynamical model of the drive for vibration analysis

The mathematical model of the rotor can be generally expressed in a matrix form in a non-rotating coordinate system

$$\boldsymbol{M}_R\ddot{\boldsymbol{q}}_R+(\omega\boldsymbol{G}_R+\boldsymbol{B}_R)\dot{\boldsymbol{q}}_R+(\boldsymbol{C}_R+\boldsymbol{K}_R)\boldsymbol{q}_R=\boldsymbol{f}_R(t), \tag{12}$$

where the matrix $\boldsymbol{M}_R$ represents the mass matrix, $\omega\boldsymbol{G}_R$ represents the gyroscopic effect matrix, $\boldsymbol{B}_R$ the damping matrix, $\boldsymbol{C}_R$ the circulation matrix and $\boldsymbol{K}_R$ the rotor stiffness matrix. The vector $\boldsymbol{q}_R$ corresponds to the vector of generalized coordinates defining the configuration space in which the mathematical model is created. The vector $\boldsymbol{f}_R(t)$ defines the external load of the rotor. The matrices listed above are obtained through the finite element method. The shaft is considered to be a one-dimensional continuum if the Euler-Bernoulli theory is adopted assuming that the cross-section area of the shaft is not distorted and remains perpendicular to the distorted axis of the shaft. This assumption can be employed in case of small distortions. Here the influence of the circulation matrix is ignored.

When modelling the rotor of an electric motor, the torsional and bending stiffness of the lamination pack is taken into account. The pack is divided into a suitable number (namely 6) of stiff discs, among which the torsional and bending stiffnesses are considered. The discs are mounted at the corresponding discretization nodes of the rotor.

The mathematical model of the rotor was further supplemented with the model of the stator so that it was possible to simulate the vibration of the stator as a result of the imbalance on the rotor [23-31]. Similarly, with respect to the rotor model, the mathematical model of the stator can generally be expressed in the matrix form

$$\boldsymbol{M}_S\ddot{\boldsymbol{q}}_S+\boldsymbol{B}_S\dot{\boldsymbol{q}}_S+\boldsymbol{K}_S\boldsymbol{q}_S=\boldsymbol{f}_S(t), \tag{13}$$

where the $\boldsymbol{M}_S$ represents the mass matrix, $\boldsymbol{B}_S$ stands for the damping matrix and $\boldsymbol{K}_S$ the stator stiffness matrix. The vector $\boldsymbol{q}_S$ corresponds to the vector of generalized coordinates defining the configuration space in which the mathematical model is created. As the stator is considered to be a rigid body fixed to the frame flexibly, the vector of the generalized coordinates is $\boldsymbol{q}_S=[x,y,z,\varphi_x,\varphi_y,\varphi_z]^T$, where the listed coordinates define the deflections of the stator centre of mass and its angular deflections the relevant coordinate axes. The vector $\boldsymbol{f}_R(t)$ defines the external load of the rotor. The

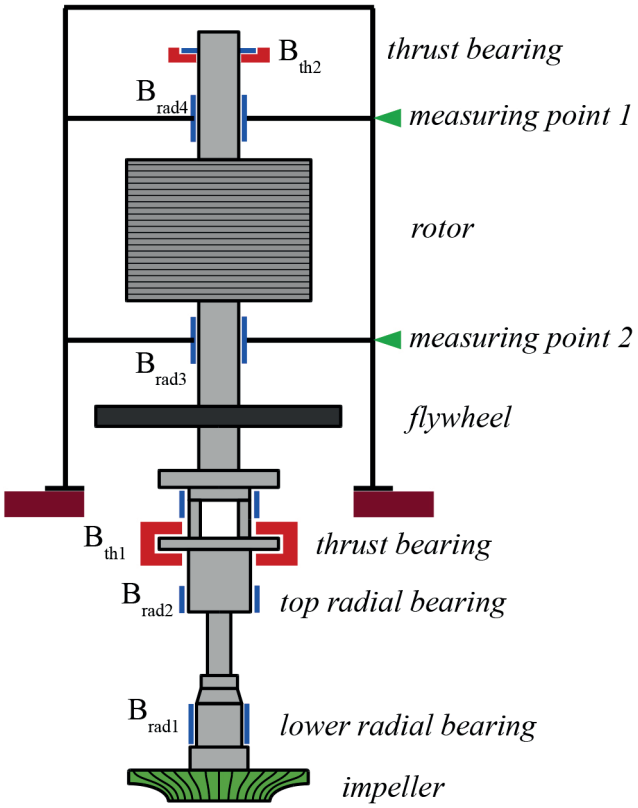

Figure 9 *Diagram of the arrangement of the machine stator and rotor*

matrices of damping and stiffness only take into account the damping and stiffness parameters of the stator fixing.

The stator and rotor are mutually coupled by means of bearings. The rotor rests on four radial and two axial journal bearings. Figure 10 shows the position of the bearings and their designation. In order to mathematically interconnect the subsystem of the rotor with the subsystem of the stator, an overall mathematical model of the system was created in the configuration space, which is defined by the vector of generalized coordinates in the form of $\boldsymbol{q} = [\boldsymbol{q}_R^T, \boldsymbol{q}_S^T]^T$. Then the complex mathematical model has following general matrix form

$$\boldsymbol{M}\dot{\boldsymbol{q}} + (\boldsymbol{B} + \boldsymbol{B}_L)\dot{\boldsymbol{q}} + (\boldsymbol{K} + \boldsymbol{K}_L)\boldsymbol{q} = \boldsymbol{f}(t). \tag{14}$$

Presented matrices can be expressed as

$$\boldsymbol{M} = \begin{bmatrix} \boldsymbol{M}_R & \boldsymbol{0} \\ \boldsymbol{0} & \boldsymbol{M}_S \end{bmatrix}, \boldsymbol{B} = \begin{bmatrix} \omega \boldsymbol{G}_R + \boldsymbol{B}_R & \boldsymbol{0} \\ \boldsymbol{0} & \boldsymbol{B}_S \end{bmatrix},$$
$$\boldsymbol{K} = \begin{bmatrix} \boldsymbol{C}_R + \boldsymbol{K}_R & \boldsymbol{0} \\ \boldsymbol{0} & \boldsymbol{K}_S \end{bmatrix} f(t) = \begin{bmatrix} \boldsymbol{f}_R(t) \\ \boldsymbol{f}_S(t) \end{bmatrix}. \tag{15}$$

Matrices $\boldsymbol{B}_L$ and $\boldsymbol{K}_L$ represent the matrices of damping and stiffness of bearing couplings. As the rotor is placed in a vertical position, the determination of the stiffness of the radial bearings is a very sophisticated problem in general. For the first approach, the stiffness of radial bearings can be estimated based on their type, their geometrical parameters and the oil viscosity according to [9]. However, this approach assumes horizontal position of the rotor and therefore the main load of the bearing is given by gravity load. Here, the main radial load is estimated based on the vertical rotor position and is determined for nominal operating speed of the rotor.

8.2 Critical speeds determination

In order to analyse basic dynamical properties of the system, especially the location of the critical speeds, the Campbell diagram was determined, i.e. the dependency of the natural frequencies on the rotor speed, see Figure 4 [7, 9, 14]. The diagram shows that the intersection point of the revolution start-up line and the curve of the second natural frequency depicted is located near the operating speed. However, this situation is not dangerous from the operational point of view because the corresponding natural shape describes the system vibration in an axial direction and therefore is not dominantly excitable due to the rotor imbalance and the unilateral magnetic pull.

The computational model created was used to determine the upper effective estimations of the radial velocities at measurement points 1 and 2, as shown in Figure 10. These spots correspond to the operational measurement points. The speed of rotor is assumed to be the nominal.

8.3 Steady-state response to imbalance forces due to rotor packet sliding

The vector of excitation forces $\boldsymbol{f}(t)$ in (14) comprises the effect of centrifugal forces. The extent of the stack bulging is simulated in

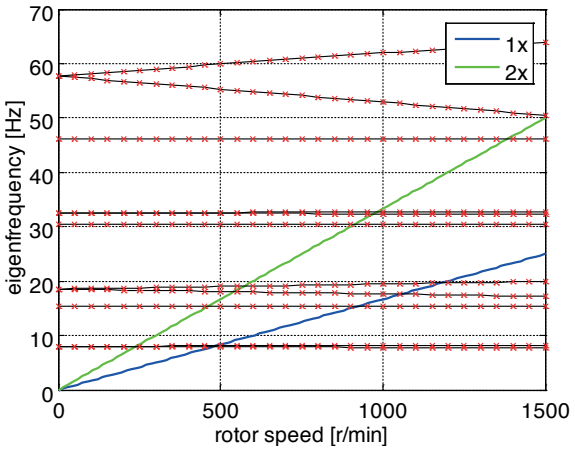

Figure 10 *Campbell diagram of the rotor-stator system*

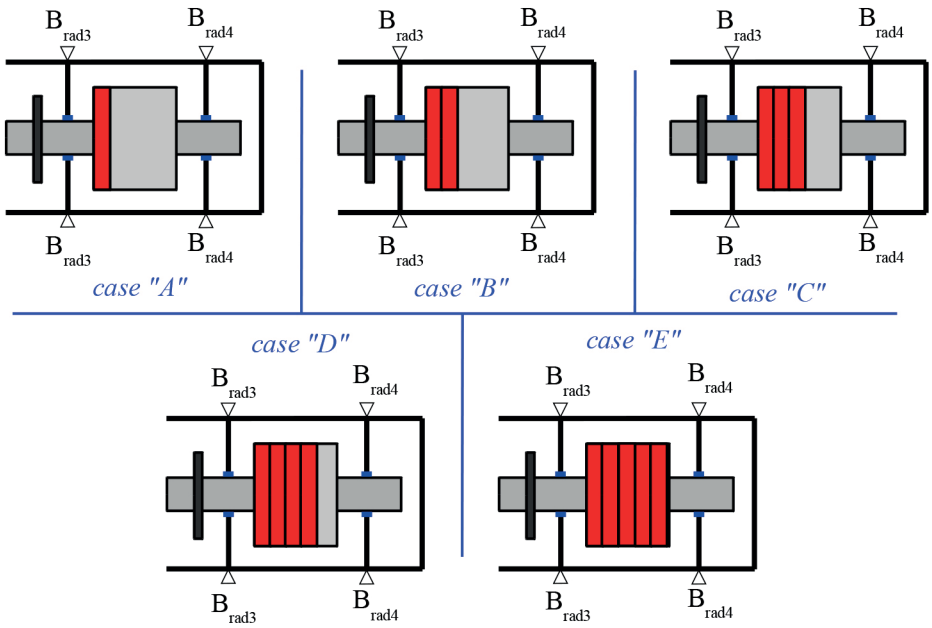

Figure 11 *Computational cases of the position of the imbalance within the rotor*

Table 3 *Determined upper effective estimations of the radial velocities at the reference points of the stator for various configurations of the considered rotor stack imbalance*

Calculation event	Upper Effective Estimation of the Velocity Amplitude in the Radial Direction [mm/s]		Location of the packet sliding
	point 2: V_{Brad3}	point 2: V_{Brad4}	
1	1.4	5.0	case “A”
2	3.1	10.4	case “B”
3	5.2	16.2	case “C”
4	7.7	22.3	case “D”
5	10.5	28.7	case “E”

a way which makes it possible to calculate the induced imbalance. Based on the findings on the rotor after its disassembling, the imbalance is given by the rotor bulging. The rotor was divided into 5 uniform segments and at each segment the imbalance due to bulging was simulated separately. The imbalance of one segment is given by the mass $\Delta m_{1/5} = 0.328\,\text{kg}$, which results in a centrifugal force of $\Delta F_{1/5} = 2.83\,\text{kN}$ under nominal speed. The computational cases of the position of the imbalance within the rotor is displayed in Figure 11. The cases were taken into account to determine what vibration level is caused by different amounts of imbalance and how it corresponds to vibration measurement.

8.4 Evaluation of vibration measurement and calculation

During the rotor operation, a vibration measurement was performed. The positions, where the vibration were recorded are designated in Figure 9 as measuring points 1 and 2. The

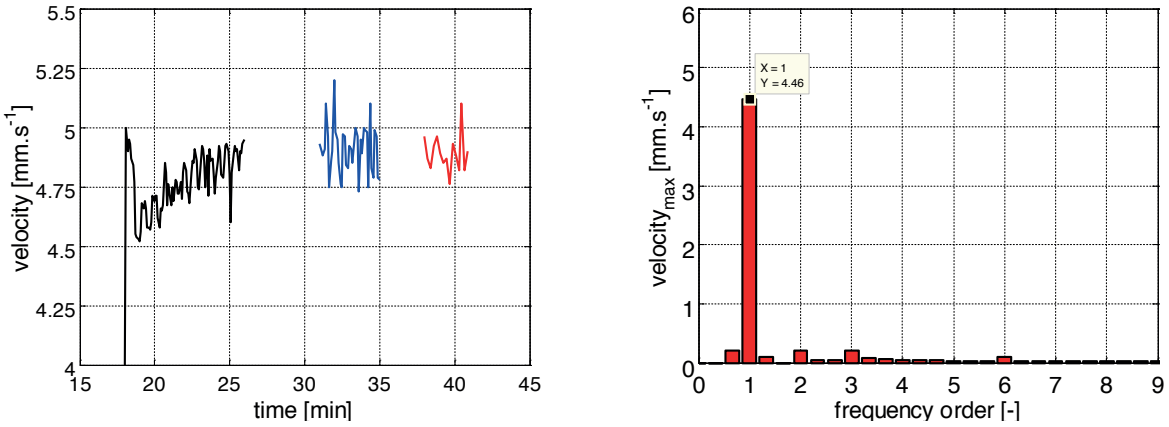

Figure 12 *Mechanical vibration measurement and FFT analysis*

measurement has been used as an indicator of vibration level of the complex equipment. The recordings (Figure 12) show that the vibration level measured by the velocity reached up to 5 mm/s, which has indicated the equipment is not capable to be operated.

The calculations were performed to confirm or disprove the source of undesirable vibration. Comparing results presented in Table 3 and measurement in Figure 12 gives good agreement for the computational case "A". It can be concluded that the amount of imbalance is given by bulging of approximately one fifth of the rotor packet. This conclusion is moreover confirmed by the frequency analysis of the measured vibration velocity. The dominant frequency contained in there corresponds to rotor spin speed frequency which gives the first order frequency (Figure 12 left).

9. Conclusion

The paper proposes a methodology how to investigate the origin of vibrations in a high performance induction motor. The methodology is based on vibration measurement and on the physical findings at the rotor after its disassembling.

In practice, the rotor vibration measurement is continuously performed on-site within a rotor diagnostic system. The vibration measurement can detect if the rotor vibration exceeds safety limits but it is not capable to decide on the vibration origin. Therefore, after analysis of the recorded vibration signal, it was found out that the dominant vibration frequency corresponds to rotor spin speed frequency. Based on that, one can conclude that the vibration source could correspond to one sided magnetic pull forces or/and to imbalance force which have the same fundamental frequency.

Based on finding after rotor disassembling, the main problem consisted in the rotor mounting, especially in its clamping. It has been found, that the improper rotor clamping resulted in rotor imbalance which further gave rise to undesirable vibrations which led to that the rotor had to be put out of operation.

The created mathematical and computational model of the machine made it possible to simulate an arbitrary imbalance of the rotor. The output of the model was the intensity of vibrations of the stator. The model was verified by a practical measurement and proved to be in very good agreement. In addition, the loosened ventilation sheet was simulated and the stress acting on it was calculated. The model predicted possible plastic distortions which were subsequently confirmed by a finding obtained after the dismantling of the machine. One of the rotor stacks exhibited an inadmissible eccentricity and the relevant ventilation sheet even suffered from a plastic deformation.

The analysis proved that an insufficient clamping force can lead to put the rotor out of operation which can finally result in high secondary financial losses, e.g. if the rotor is operated primary circuit within nuclear power plants.

Acknowledgement

This research has been supported by the Ministry of Education, Youth and Sports of the Czech Republic under the RICE - New Technologies and Concepts for Smart Industrial Systems, project No. LO1607 and by funding program of the University of West Bohemia number SGS-2018-009.

References

[1] FINLEY, W., LOUTFI, M. SAUER, B. J. Motor vibration problems - Understanding and identifying. In *2013 IEEE-IAS/PCA Cement Industry Technical Conference : proceedings* [online]. Orlando, FL, USA, 2013, p. 1-20. Available from: https://doi.org/10.1109/CITCON.2013.6525282

[2] MISTRY, R., et al. Influencing factors on motor vibration & rotor critical speed in design, test and field applications. In 2014 IEEE Petroleum and Chemical Industry Technical Conference (PCIC) *Conference : proceedings* [online]. *San Francisco, CA, USA, 2014,* p. 227-236. Available from: https://doi.org/10.1109/PCICon.2014.6961887

[3] YAMAZAKI, K., WATANABE, Y. Interbar current analysis of induction motors using 3-D finite-element method considering lamination of rotor core. *IEEE Transactions on Magnetics* [online]. 2006, **42**(4), p. 1287-1290. ISSN 0018-9464. Available from: https://doi.org/10.1109/TMAG.2006.871423

[4] FERKOVA, Z. Comparison of two-phase induction motor modeling in ANSYS Maxwell 2D and 3D program. In 10th International Conference ELEKTRO 2014 *: proceedings*. Zilina: Faculty of Electrical Engineering, 2014, p. 279-284.

[5] KALAMEN, L., et al. A novel method of magnetizing inductance investigation of self-excited induction generators. *IEEE Transactions on Magnetics* [online]. 2012, 48(4), p. 1657-1660. ISSN 0018-9464. Available from: https://doi.org/10.1109/TMAG.2011.2173312

[6] PYRHONEN, J., et al. Harmonic loss calculation in rotor surface permanent magnets - New analytic approach. *IEEE Transactions on Magnetics* [online]. 2012, 48(8), p. 2358-2366. ISSN 0018-9464. Available from: https://doi.org/10.1109/TMAG.2012.2190518

[7] MARQUES CARDOSO, A. J., et al. Rotor cage fault diagnosis in three-phase induction motors, by Park's vector approach. IAS '95. Conference Record of the 1995 IEEE Industry Applications Conference Thirtieth IAS Annual Meeting : *proceedings* [online]. Vol. 1. Orlando, FL, USA, 1995, p. 642-646. ISBN 0-7803-3008-0/ISSN 0197-2618. Available from: https://doi.org/10.1109/IAS.1995.530360

[8] BINDU, S., THOMAS, V. V. Diagnoses of internal faults of three phase squirrel cage induction motor - A review. In 2014 International Conference on Advances in Energy Conversion Technologies (ICAECT) : *proceedings* [online]. Manipal, India, 2014, p. 48-54. Available from: https://doi.org/10.1109/ICAECT.2014.6757060

[9] NAHA, A., et al. A method for detecting half-broken rotor bar in lightly loaded induction motors using current. *IEEE Transactions on Instrumentation and Measurement* [online]. 2016, **65**(7), p. 1614-1625. ISSN 0018-9456. Available from: https://doi.org/10.1109/TIM.2016.2540941

[10] VALLES-NOVO, R., et al. Empirical mode decomposition analysis for broken-bar detection on squirrel cage induction motors. *IEEE Transactions on Instrumentation and Measurement* [online]. 2015, **64**(5), p. 1118-1128. ISSN 0018-9456. Available from: https://doi.org/10.1109/TIM.2014.2373513

[11] SOUALHI, A., CLERC, G., RAZIK, H. Detection and diagnosis of faults in induction motor using an improved artificial ant clustering technique. *IEEE Transactions on Industrial Electronics* [online]. 2013, **60**(9), p. 4053-4062. ISSN 0278-0046/eISSN 1557-9948. Available from: https://doi.org/10.1109/TIE.2012.2230598

[12] CEBAN, A., PUSCA, R., ROMARY, R. Study of rotor faults in induction motors using external magnetic field analysis. *IEEE Transactions on Industrial Electronics* [online]. 2012, **59**(5), p. 2082-2093. ISSN 0278-0046/eISSN 1557-9948. Available from: https://doi.org/10.1109/TIE.2011.2163285

[13] ROMERO-TRONCOSO, R. J., et al. FPGA-based online detection of multiple combined faults in induction motors through information entropy and fuzzy inference. *IEEE Transactions on Industrial Electronics* [online]. 2011, 58(11), p. 5263-5270. ISSN 0278-0046/eISSN 1557-9948. Available from: https://doi.org/10.1109/TIE.2011.2123858

[14] KIA, S. H., HENAO, H., CAPOLINO, G. A. A high-resolution frequency estimation method for three-phase induction machine fault detection. *IEEE Transactions on Industrial Electronics* [online]. 2007, **54**(4), p. 2305-2314. ISSN 0278-0046/eISSN 1557-9948. Available from: https://doi.org/10.1109/TIE.2007.899826

[15] RANGEL-MAGDALENO, J. d. J., et al. Novel methodology for online half-broken-bar detection on induction motors. *IEEE Transactions on Instrumentation and Measurement* [online]. 2009, 58(5), p. 1690-1698. ISSN 0018-9456. Available from: https://doi.org/10.1109/TIM.2009.2012932

[16] OJAGHI, M., NASIRI, S. Dynamic simulation of eccentric squirrel cage induction motors by including saturable reluctances of individual teeth. *IET Electric Power Applications* [online]. 2014, **8**(6), p. 232-239. ISSN 1751-8660/eISSN 1751-8679. Available from: https://doi.org/10.1049/iet-epa.2013.0381

[17] BERNAT, P., KACOR, P. Operational non-contact diagnostics of induction machine based on stray electromagnetic field. *Communications - Scientific Letters of the University of Zilina* [online]. 2015, **17**(1A), p. 89-94. ISSN 1335-4205/eISSN 2585-7878. Available from: http://komunikacie.uniza.sk/index.php/communications/article/view/418

[18] ORSAG, O., et al. Influence of rotor slot shape on the parameters of induction motor. IEEE International Conference on Environment and Electrical Engineering and IEEE Industrial and Commercial Power Systems Europe (EEEIC/I&CPS Europe 2017) : proceedings [online]. Milan, Italy, 2017. ISBN 978-1-5386-3916-0. p. 1-6. Available from: https://doi.org/10.1109/EEEIC.2017.7977673

[19] BANGURA, J. F., et al. Diagnostics of eccentricities and bar/end-ring connector breakages in polyphase induction motors through a combination of time-series data mining and time-stepping coupled FE-state-space techniques. *IEEE Transactions on Industry Applications* [online]. 2003, **39**(4), p. 1005-1013. ISSN 0093-9994/eISSN 1939-9367. Available from: https://doi.org/10.1109/TIA.2003.814582

[20] JOKSIMOVIC, G. M. Dynamic simulation of cage induction machine with air gap eccentricity. *IEE Proceedings - Electric Power Applications* [online]. 2005, **152**(4), p. 803-811. ISSN 1350-2352/eISSN 1359-7043. Available from: https://doi.org/10.1049/ip-epa:20041229

[21] SILWAL, P., et al. Numerical analysis of the power balance of an electrical machine with rotor eccentricity. *IEEE Transactions on Magnetics* [online]. 2016, **52**(3), p. 1-4. ISSN 0018-9464. Available from: https://doi.org/10.1109/TMAG.2015.2477847

[22] PYRHONEN, J., JOKINEN, T., HRABOVCOVA, V. Design of rotating electrical machines. Wiley, 2014. ISBN 978-1-118-58157-5

[23] OBAID, R. R., HABETLER, T. G., GRITTER, D. J. A simplified technique for detecting mechanical faults using stator current in small induction motors. 2000 IEEE Industry Applications Conference, Thirty-Fifth IAS Annual Meeting and World Conference on Industrial Applications of Electrical Energy : conference record [online]. Vol. 1. Rome, Italy, 2000. ISBN 0-7803-6401-5/ISSN 0197-2618, p. 479-483. Available from: https://doi.org/10.1109/IAS.2000.881153

[24] KOSTIC-PEROVIC, D., ARKAN, M., UNSWORTH, P. Induction motor fault detection by space vector angular fluctuation. 2000 IEEE Industry Applications Conference, Thirty-Fifth IAS Annual Meeting and World Conference on Industrial Applications of Electrical Energy: conference record [online]. Vol. 1. Rome, Italy, 2000. ISBN 0-7803-6401-5/ISSN 0197-2618, p. 388-394. Available from: https://doi.org/10.1109/IAS.2000.881140

[25] ELKASABGY, N. M., EASTHAM, A. R., DAWSON, G. E. Detection of broken bars in the cage rotor on an induction machine. *IEEE Transactions on Industry Applications* [online]. 1992, **28**(1), p. 165-171. ISSN 0093-9994/eISSN 1939-9367. Available from: https://doi.org/10.1109/28.120226

[26] CAMERON, J. R., THOMSON, W. T., DOW, A. B. Vibration and current monitoring for detecting airgap eccentricity in large induction motors. *IEE Proceedings B - Electric Power Applications* [online]. 1986, **133**(3), p. 155-163. ISSN 0143-7038/eISSN 2053-7913. Available from: https://doi.org/10.1049/ip-b:19860022

[27] DORRELL, D. G., THOMSON, W. T., ROACH, S. Analysis of airgap flux, current, and vibration signals as a function of the combination of static and dynamic airgap eccentricity in 3-phase induction motors. *IEEE Transactions on Industry Applications* [online]. 1997, **33**(1), p. 24-34. ISSN 0093-9994/eISSN 1939-9367. Available from: https://doi.org/10.1109/28.567073

[28] NANDI, S. AHMED, S., TOLIYAT, H. A. Detection of rotor slot and other eccentricity related harmonics in a three phase induction motor with different rotor cages. *IEEE Transactions on Energy Conversion* [online]. 2001, **16**(3), p. 253-260. ISSN 0885-8969. Available from: https://doi.org/10.1109/60.937205

[29] TOLIYAT, H. A., AREFEEN, M. S., PARLOS, A. G. A method for dynamic simulation of air-gap eccentricity in induction machines. *IEEE Transactions on Industry Applications* [online]. 1996, **32**(4), p. 910-918. ISSN 0093-9994/eISSN 1939-9367. Available from: https://doi.org/10.1109/28.511649

[30] CARDOSO, J. M., SARAIVA, E. S. Computer-aided detection of airgap eccentricity in operating three-phase induction motors by Park's vector approach. *IEEE Transactions on Industry Applications* [online]. 1993, **29**(5), p. 897-901. ISSN 0093-9994/eISSN 1939-9367. Available from: https://doi.org/10.1109/28.245712

[31] AL-NUAIM, N. A., TOLIYAT, H. A novel method for modeling dynamic air-gap eccentricity in synchronous machines based on modified winding function theory. *IEEE Transactions on Energy Conversion* [online]. 1998, **13**(2), p. 156-162. ISSN 0885-8969. Available from: https://doi.org/10.1109/60.678979

[32] BONNETT, A. H., SOUKUP, G. C. Analysis of rotor failures in squirrel-cage induction motors. *IEEE Transactions on Industry Applications* [online]. 1988, **24**(6), p. 1124-1130. ISSN 0093-9994/eISSN 1939-9367. Available from: https://doi.org/10.1109/28.17488

[33] BOGH, D., CROWELL, J., AMSTUTZ, R. IEEE 841 motor vibration. *IEEE Industry Applications Magazine* [online]. 2005, **11**(6), p. 32-37. ISSN 1077-2618. Available from: https://doi.org/10.1109/MIA.2005.1524734

[34] STACK, J. R., HABETLER, T. G., HARLEY, R. G. Effects of machine speed on the development and detection of rolling element bearing faults. *IEEE Power Electronics Letters* [online]. 2003, **1**(1), p. 19-21. ISSN 1540-7985/eISSN 1558-3767. Available from: https://doi.org/10.1109/LPEL.2003.814607

[35] BANGURA, J. F., et al. Diagnostics of eccentricities and bar/end-ring connector breakages in polyphase induction motors through a combination of time-series data mining and time-stepping coupled FE-state-space techniques. *IEEE Transactions on Industry Applications* [online]. 2003, **39**(4), p. 1005-1013. ISSN 1077-2618. Available from: https://doi.org/10.1109/TIA.2003.814582

[36] OBAID, R. R., HABETLER, T. G., GRITTER, D. J. A simplified technique for detecting mechanical faults using stator current in small induction motors. 2000 IEEE Industry Applications Conference. Thirty-Fifth IAS Annual Meeting and World Conference on Industrial Applications of Electrical Energy : conference record [online]. Vol. 1. Rome, Italy, 2000. ISBN 0-7803-6401-5/ISSN 0197-2618, p. 479-483. Available from: https://doi.org/10.1109/IAS.2000.881153

[37] DEN HARTOG, J. P. Advanced Strength of Materials. Dover Civil Mechanical Engineering, Dover Publications, 1987. ISBN 978-0486654072.